

Search for Quantum Decoherence in Neutrino Oscillations with KM3NeT ORCA6

Nadja Lessing^{a,*} on behalf of the KM3NeT Collaboration

^a*Instituto de Física Corpuscular IFIC (CSIC - Universidad de Valencia),
Parque Científico Catedrático José Beltrán 2, Paterna, Spain*

E-mail: Nadja.Lessing@ific.uv.es

Quantum decoherence of neutrino states is an effect that is proposed in various theories of quantum gravity. It is envisaged to emerge from interactions of the neutrino as a quantum system with the environment and may destroy the superposition of neutrino mass states, which leads to a modification of neutrino oscillation probabilities.

KM3NeT/ORCA, a neutrino telescope designed to detect various neutrino flavours across a broad spectrum of energies, can probe this phenomenon. ORCA is a water Cherenkov detector that is currently under construction in the Mediterranean Sea. It was designed to detect atmospheric neutrinos in the GeV energy range. The main objective of ORCA is the precise measurement of neutrino oscillations. Therefore, the detector provides the possibility to investigate various beyond Standard Model scenarios that may alter the oscillation pattern.

This contribution reports on first constraints on the strength of decoherence effects with KM3NeT. We provide upper limits on the decoherence parameters γ_{21} and γ_{31} . The high-purity neutrino sample used for this analysis was collected with a six Detection Units configuration of ORCA with an exposure of 433 kton-years.

POS(ICRC2023) 1025

38th International Cosmic Ray Conference (ICRC2023)
26 July - 3 August, 2023
Nagoya, Japan



*Speaker

1. The KM3NeT detectors

The KM3NeT research infrastructure comprises two water Cherenkov detectors which are currently under construction in the Mediterranean sea. These detectors, known as KM3NeT/ARCA and KM3NeT/ORCA are composed of 3D arrays of Digital Optical Modules arranged in vertical Detection Units. Each of the modules hosts 31 Photomultiplier tubes which collect Cherenkov light emitted by the charged particles produced in neutrino interactions. ORCA is optimized to detect atmospheric neutrinos in the GeV energy range and to precisely measure the neutrino oscillation parameters. In the final configuration the ORCA detector will encompass 115 Detection Units yielding a total instrumented volume of 7 Mton of sea water. The data analyzed for this proceeding was recorded between February 2020 and November 2021 with a configuration of 6 Detection Units, which we refer to as ORCA6 in the following. The total lifetime is 510 days which results in an exposure of 433 kton-years.

2. Theory of decoherence in neutrino oscillations

Neutrino oscillations are considered coherent because the different mass eigenstates maintain their relative phase relationships as they propagate. However, neutrino eigenstates may loose their quantum superposition in a phenomenon known as neutrino decoherence. In this analysis, we consider *non-standard* decoherence, induced by the coupling of the neutrino as a quantum system with the environment. The time evolution of the neutrino system including decoherence effects is described by adding a non-unitary term to the Liouville–von Neumann equation [1]

$$\frac{d}{dt}\rho = -i[H, \rho] - \mathcal{D}[\rho], \quad (1)$$

where ρ is the density matrix of the neutrino and H is the full Hamiltonian in matter. With the condition of complete positivity of the time evolution and trace conservation, the decoherence term can be written in the so-called *Lindblad* form [2]

$$\mathcal{D}[\rho] = \sum_m (\{\rho, D_m D_m^\dagger\} - 2D_m \rho D_m^\dagger), \quad (2)$$

where the D_m are complex matrices, with the index $m \in [1, N^2 - 1]$ where N is the dimension of the $SU(N)$ Hilbert space of the neutrino system. The D_m are required to be Hermitian which implies increasing entropy. The condition of complete positivity ensures that the eigenvalues of ρ remain positive which is crucial for their interpretation as probabilities. Assuming energy conservation in the effective mass basis, the D_m and H can be diagonalized simultaneously with $\tilde{H} = \text{diag}(\tilde{E}_1, \tilde{E}_2, \tilde{E}_3)$ describing the energy in the effective mass basis. The solution of Equation 1 for three neutrino families in uniform matter is given by

$$\tilde{\rho}_{ij} = \tilde{\rho}_{ij}(0) e^{-i\Delta\tilde{E}_{ij}t - \gamma_{ij}t}, \quad i, j = 1, 2, 3 \quad (3)$$

where $\tilde{\rho}$ is the density matrix in the effective mass basis, $\tilde{\rho}_{ij}(0)$ is determined by the initial conditions and $\Delta\tilde{E}_{ij} = \tilde{E}_i - \tilde{E}_j$ describes the difference in the total neutrino energies. Additionally, we introduced the decoherence parameter defined by

$$\gamma_{ij} = \sum_m (d_m^i - d_m^j)^2, \quad (4)$$

where the d_m^i are the entries of the diagonalized matrices D_m . We assume that the d_m^i are constant and independent of matter effects, following the approach in [2]. It is important to note that this does not imply that decoherence effects themselves are independent of matter effects. For this analysis we use atmospheric neutrinos that traverse the Earth before being detected. In order to apply Equation 3 the Earth is modeled by 15 layers of constant density. In presence of decoherence effects the oscillation probabilities are calculated via

$$P(\nu_\alpha \rightarrow \nu_\beta) = \sum_{i,j} \tilde{U}_{\alpha i} \tilde{U}_{\beta i}^* \tilde{U}_{\alpha j}^* \tilde{U}_{\beta j} e^{-i\Delta\tilde{E}_{ij}t - \gamma_{ij}t}, \quad (5)$$

where \tilde{U} is the diagonalized Pontecorvo-Maki-Nakagawa-Sakata matrix. The only difference to standard neutrino oscillations is the presence of a damping term $e^{-\gamma_{ij}t}$. The common approach in decoherence studies is to assume that the decoherence parameter may depend on the neutrino energy as

$$\gamma_{ij} = \gamma_{ij}^0 \left(\frac{E}{\text{GeV}} \right)^n. \quad (6)$$

In this work we consider $n = -2, -1$ since these cases affect lower energies that ORCA is most sensitive to. As can be seen from Equation 4 the decoherence parameters are not independent of each other. Consequently, we provide upper limits on γ_{21} and γ_{31} as, under the most conservative assumptions for our experiment, the third parameters is fixed by [3]

$$\gamma_{32} = \gamma_{31} + \gamma_{21} - 2\sqrt{\gamma_{21}\gamma_{31}}. \quad (7)$$

3. Analysis methods

This analysis employs a binned log-likelihood minimization technique to compare the data to the Monte Carlo expectation. The nominal values of the oscillation parameters as given in Table 1 are provided by Nu-Fit 5.0 [5]. The data is reconstructed in 2D event histograms of the energy and zenith angle with a binning scheme that ensures an expectation of at least two events per bin. The negative likelihood function is minimized for θ_{23} , Δm_{31}^2 , and a set of nuisance parameters described in detail in [6]. The nuisance parameters along with their corresponding prior uncertainties are summarized in Table 2. The prior uncertainties are assumed to be Gaussian distributed.

Parameter	Nominal value NO	Nominal value IO	Treatment
Δm_{31}^2 [eV ²]	$2.517 \cdot 10^{-3}$	$-2.424 \cdot 10^{-3}$	free
Δm_{21}^2 [eV ²]	$7.42 \cdot 10^{-5}$	$7.42 \cdot 10^{-5}$	fixed
θ_{12} [°]	33.44	33.45	fixed
θ_{13} [°]	8.57	8.60	fixed
θ_{23} [°]	49.2	49.3	free
δ_{CP} [°]	197	282	fixed

Table 1: Oscillation parameters for normal ordering (NO) and inverted ordering (IO) with their treatment in the minimization.

Only data from periods characterized by high stability in environmental conditions as well as data acquisition were used in this analysis, which results in an exposure of 433 kton-years.

Cuts based on the trigger rate and the reconstruction quality efficiently reject background events from pure noise. The analysis is restricted to up-going events which significantly reduces the atmospheric muon background. Two Boosted Decision Trees (BDT) are employed to effectively discriminate against atmospheric muons and to differentiate between track-like and shower-like events. Additional cuts on the atmospheric muon BDT score further reduce the atmospheric muon contamination to below 5 %. This result in a total of 5828 observed events. These events are divided into three classes in order to optimize the sensitivity: a high purity tracks class with negligible muon contamination, a low purity tracks class and a showers class. The tracks classes contain events with reconstructed energies between 2 GeV and 100 GeV, whereas the showers class ranges from 2 GeV to 1 TeV.

More information on the selected data set can be found in the proceedings for measuring atmospheric neutrino oscillation with KM3NeT/ORCA6 [7].

Parameter	Prior
Spectral index	± 0.3
Energy scale	$\pm 9\%$
$\nu_{\text{hor}}/\nu_{\text{ver}}$ ratio	$\pm 2\%$
$\nu_e/\bar{\nu}_e$ ratio	$\pm 7\%$
$\nu_\mu/\bar{\nu}_\mu$ ratio	$\pm 5\%$
$(\nu_\mu + \bar{\nu}_\mu)/(\nu_e + \bar{\nu}_e)$ ratio	$\pm 2\%$
High-energy light simulation	$\pm 50\%$
NC normalization	$\pm 20\%$
τ -CC normalization	$\pm 20\%$
Muon normalization	free
Track normalization	free
Showers normalization	free
Overall normalization	free

Table 2: Nuisance parameters along with their prior uncertainties.

4. Results

Fitting the data, no significant deviation was found with respect to the standard oscillation analysis. The fitted values of γ_{21} and γ_{31} are consistent with zero. Figure 1 shows the difference in the log-likelihood ratios of decoherence and standard oscillations in dependence of the reconstructed energy and zenith angle at the best fit values $\gamma_{ij,\text{BF}}$ for the high purity tracks class. For $\gamma \propto E^{-2}$ (left) the red bins give a better fit for decoherence while the blue bins are in better agreement with standard oscillations. For $\gamma \propto E^{-1}$ (right) there is no difference with respect to the standard oscillations best fit.

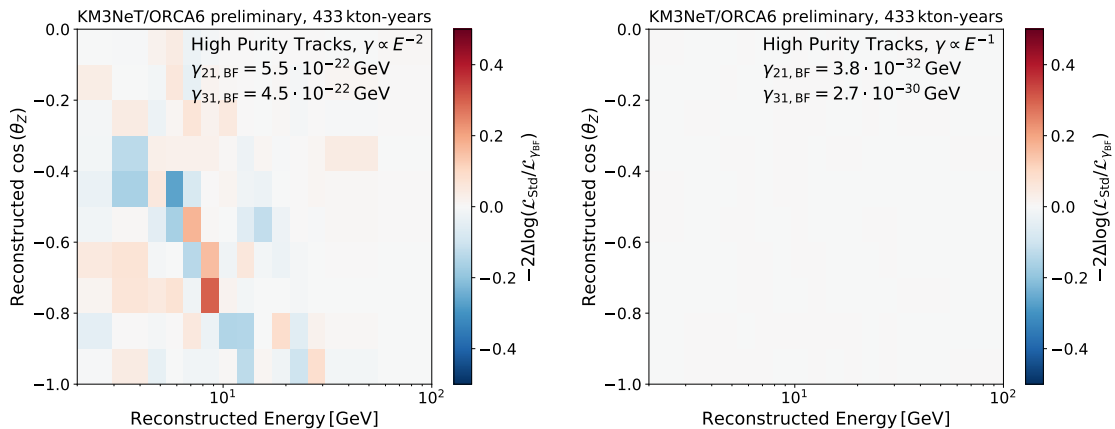


Figure 1: Difference in the log-likelihood ratios of decoherence and standard oscillations at the best fit for the high purity tracks class for $\gamma \propto E^{-2}$ (left) and $\gamma \propto E^{-1}$ (right).

The upper limits on γ are determined by computing the log-likelihood ratio with respect to the global best fit as a function of one decoherence parameter while leaving the other parameter free in the minimization. By exploring the full parameter space and allowing for non-zero values of all three decoherence parameters, the most conservative limits are obtained. Furthermore, the minimization is performed for both octants of θ_{23} and for both neutrino mass orderings.

The solid curves in Figure 2 show the log-likelihood ratio as a function of γ_{21} and γ_{31} for each of the energy dependencies $\gamma \propto E^{-2}$ (left) and $\gamma \propto E^{-1}$ (right). Additionally, the blue dashed line shows the log-likelihood ratio for γ_{21} assuming normal ordering (NO). For small values of γ_{21} normal ordering is preferred whereas for large values of γ_{21} inverted ordering (IO) gives the minimal log-likelihood ratio. The upper limits at the 95% CL are presented in Figure 3 for both, NO and IO. This figure illustrates how the limits strongly depend on the considered mass ordering which emphasizes the importance of performing the minimization for both cases.

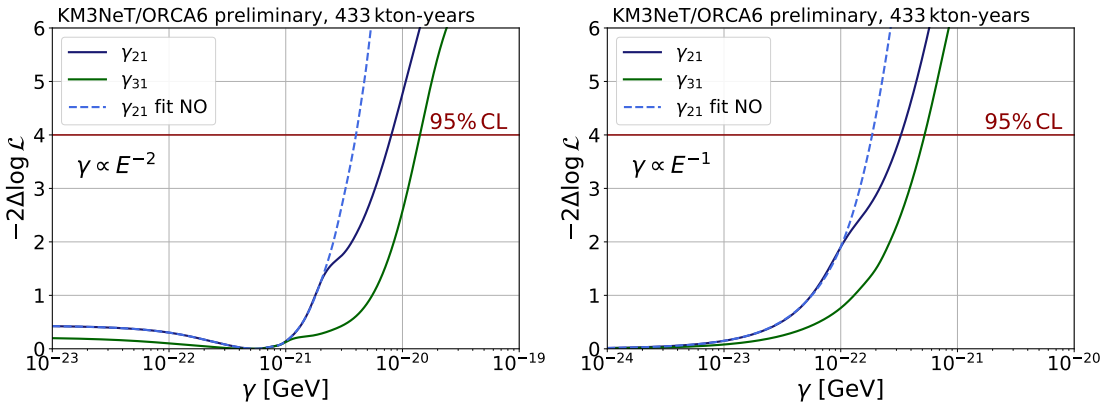


Figure 2: Log-likelihood ratio with respect to the global best fit for $\gamma \propto E^{-2}$ (left) and $\gamma \propto E^{-1}$ (right) as a function of the decoherence parameters γ_{21} and γ_{31} . The solid lines were obtained fitting both, normal and inverted ordering, as well as both octants of θ_{23} and keeping the overall best fit. The blue dashed line was obtained assuming normal ordering.

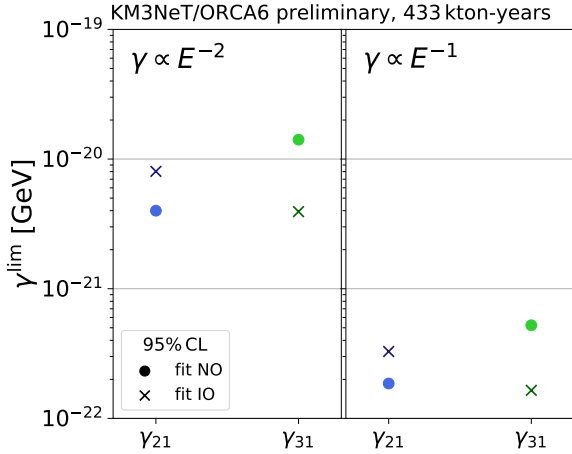


Figure 3: Upper limits on γ_{21} and γ_{31} at the 95% CL assuming NO (dots) and IO (crosses).

[Figure 4](#) shows CL contours which serve to constrain both decoherence parameters γ_{21} and γ_{31} at the same time. The log-likelihood ratio is small along the diagonal since for $\gamma_{21} = \gamma_{31} \Rightarrow \gamma_{32} = 0$. The irregular shape of the curves is caused by a flip in the best fit mass ordering. This is evident from [Figure 5](#) which depicts the 95 % confidence level contour assuming either NO or IO as well as considering both mass orderings. As already seen in the one-dimensional profiles, the upper limits differ greatly depending on the mass ordering.

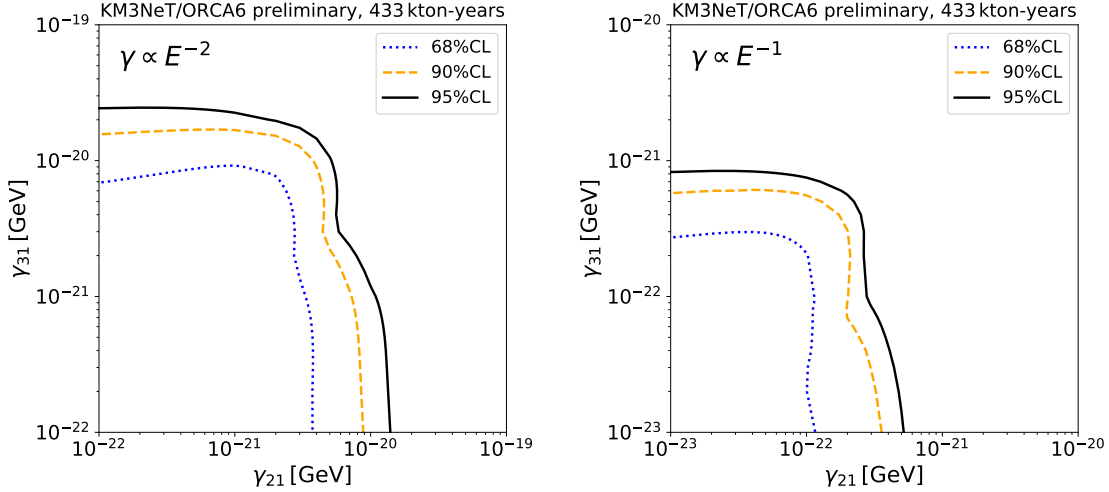


Figure 4: Confidence level contours of γ_{31} and γ_{21} for $\gamma \propto E^{-2}$ (left) and $\gamma \propto E^{-1}$ (right). The upper right part of the plane is excluded for each model at the corresponding CL.

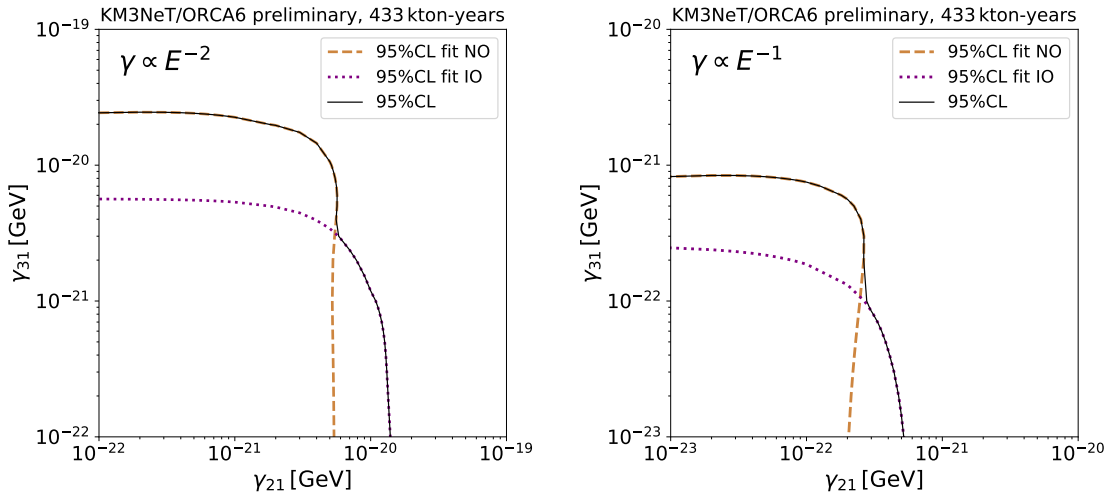


Figure 5: 95% CL contours of γ_{31} and γ_{21} assuming NO (brown dashed), assuming IO (purple dotted) and fitting both mass orderings (black solid).

Figure 6 shows the difference in the log-likelihood ratio of decoherence and standard oscillations for $\gamma \propto E^{-2}$ (left) and $\gamma \propto E^{-1}$ (right) with the decoherence parameters at the respective 95% CL upper limit for each model, and with $\gamma_{21} = \gamma_{31}$. The blue bins correspond to a better fit of standard oscillations than decoherence at the given values of γ and therefore serve to exclude decoherence effects. It can be seen that the most relevant bins are centered around 10 GeV for both models but extend towards slightly higher energies for the $\gamma \propto E^{-1}$ model.

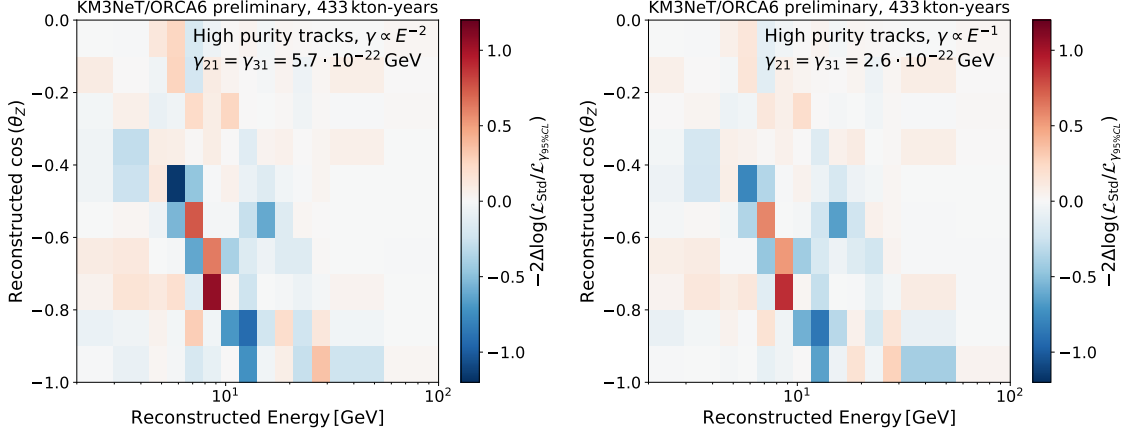


Figure 6: Difference in the log-likelihood ratios of decoherence and standard oscillations for $\gamma \propto E^{-2}$ (left) and $\gamma \propto E^{-1}$ (right) with the decoherence parameters fixed at the respective 95% CL upper limit with $\gamma_{21} = \gamma_{31}$. The blue bins serve to exclude decoherence since they correspond to a better fit of standard oscillations than decoherence.

Upper limits in GeV	$\gamma \propto E^{-2}$		$\gamma \propto E^{-1}$	
	NO	IO	NO	IO
ORCA6 (this work)				
γ_{21}	$3.0 \cdot 10^{-21}$	$5.2 \cdot 10^{-21}$	$1.3 \cdot 10^{-22}$	$1.8 \cdot 10^{-22}$
γ_{31}	$10.3 \cdot 10^{-21}$	$2.9 \cdot 10^{-21}$	$3.5 \cdot 10^{-22}$	$1.0 \cdot 10^{-22}$
$\gamma_{21} = \gamma_{31}$	$4.5 \cdot 10^{-21}$	$3.2 \cdot 10^{-21}$	$2.1 \cdot 10^{-22}$	$1.2 \cdot 10^{-22}$
Reported in [4]				
$\gamma_{21} = \gamma_{32}$	$7.9 \cdot 10^{-27}$ (KL)	-	$1.8 \cdot 10^{-24}$ (KL)	-
$\gamma_{31} = \gamma_{32}$	$6.9 \cdot 10^{-25}$ (R)	-	$2.1 \cdot 10^{-23}$ (T2K)	-
$\gamma_{21} = \gamma_{31}$	$7.9 \cdot 10^{-27}$ (KL)	-	$1.8 \cdot 10^{-24}$ (KL)	-

Table 3: Upper limits at the 90 % CL for ORCA6 in comparison with the most constraining upper limits reported in [4] using data from KamLAND (KL), RENO (R) and T2K. Note that in [4] one of the decoherence parameters is set to zero whereas in this work for the limit on γ_{21} (γ_{31}) the other parameter γ_{31} (γ_{21}) is left free in the fit in order to obtain the most conservative limits.

In general, comparing to results from other analyses is not straightforward since the assumptions on the model and the procedure used to obtain upper limits differ. Nevertheless, **Table 3** summarizes recent upper limits reported in [4] using data from KamLAND, RENO and T2K along with the values obtained in this analysis for ORCA6. It is important to note that in our analysis, when setting

a limit on γ_{21} (γ_{31}) the other parameter γ_{31} (γ_{21}) is left free in the fit whereas [4] considers limiting cases of decoherence where one of the parameters is set to zero, so the other two are equal. The same applies for the upper limits reported in [2] using three years of DeepCore data. Still, our limit on γ_{21} (γ_{31}) is approximately comparable to the case $\gamma_{21} = \gamma_{32}$ ($\gamma_{31} = \gamma_{32}$) since the decoherence parameters that is left free in the fit tends to be at least one order of magnitude smaller.

Upper limits in GeV	$\gamma \propto E^{-2}$		$\gamma \propto E^{-1}$	
	NO	IO	NO	IO
ORCA6 (this work)				
γ_{21}	$4.0 \cdot 10^{-21}$	$8.0 \cdot 10^{-21}$	$1.9 \cdot 10^{-22}$	$3.3 \cdot 10^{-22}$
γ_{31}	$14.6 \cdot 10^{-21}$	$3.9 \cdot 10^{-21}$	$5.2 \cdot 10^{-22}$	$1.6 \cdot 10^{-22}$
$\gamma_{21} = \gamma_{31}$	$5.7 \cdot 10^{-21}$	$3.9 \cdot 10^{-21}$	$2.6 \cdot 10^{-22}$	$1.6 \cdot 10^{-22}$
DeepCore	NO	IO	NO	IO
$\gamma_{21} = \gamma_{32}$	$7.5 \cdot 10^{-21}$	$5.0 \cdot 10^{-20}$	$3.5 \cdot 10^{-22}$	$2.3 \cdot 10^{-21}$
$\gamma_{31} = \gamma_{32}$	$4.3 \cdot 10^{-20}$	$1.4 \cdot 10^{-20}$	$2.0 \cdot 10^{-21}$	$5.8 \cdot 10^{-22}$
$\gamma_{21} = \gamma_{31}$	$1.2 \cdot 10^{-20}$	$8.3 \cdot 10^{-21}$	$5.4 \cdot 10^{-22}$	$3.6 \cdot 10^{-22}$

Table 4: Upper limits on the decoherence parameters at the 95 % CL for ORCA6 in comparison with results reported in [2] using DeepCore data.

5. Conclusions

We provided first constraints on neutrino decoherence effects using data from the KM3NeT/ORCA detector. Both octants of θ_{23} and both neutrino mass orderings were taken into account to derive the most conservative upper limits on the decoherence parameters. Also, we allowed all three decoherence parameters to take non-zero values and explored the full parameter space by computing confidence level contours of γ_{21} and γ_{31} . Our results have demonstrated that even with only six Detection Units, the ORCA detector is capable of providing limits on decoherence effects that are comparable to those of other analyses. This allows to anticipate the potential of the full ORCA detector which will consist of 115 Detection Units and will be able to give more stringent limits.

References

- [1] G. Lindblad., DOI: 10.1007/BF01608499 (1976)
- [2] P. Coloma et al., DOI: 10.1140/epjc/s10052-018-6092-6 (2018)
- [3] G. Balieiro Gomes et al., DOI: 10.1103/PhysRevD.100.055023 (2019)
- [4] V. De Romeri et al., arXiv:2306.14699 (2023)
- [5] Esteban et al., DOI: 10.1007/JHEP09(2020)178 (2020)
- [6] The KM3NeT Collaboration, DOI: 10.1140/epjc/s10052-021-09893-0 (2022)
- [7] V. Carretero for the KM3NeT Collaboration, PoS **ICRC2023** 996 (these proceedings)

Full Authors List: The KM3NeT Collaboration

S. Aiello^a, A. Albert^{b,bd}, S. Alves Garre^c, Z. Aly^d, A. Ambrosone^{f,e}, F. Ameli^g, M. Andre^h, E. Androutsouⁱ, M. Anguita^j, L. Aphectche^k, M. Ardid^l, S. Ardid^l, H. Atmani^m, J. Aublinⁿ, L. Bailly-Salins^o, Z. Bardačová^{q,p}, B. Baretⁿ, A. Bariego-Qintana^c, S. Basegmez du Pree^r, Y. Becheriniⁿ, M. Bendahman^{m,n}, F. Benfenati^{t,s}, M. Benhassi^{u,e}, D. M. Benoit^v, E. Berbee^r, V. Bertin^d, S. Biagi^w, M. Boettcher^x, D. Bonanno^w, J. Boumaaza^m, M. Bouda^y, M. Bouwhuis^r, C. Bozza^{z,e}, R. M. Bozza^{f,e}, H. Brâncăs^{aa}, F. Bretaudeau^k, R. Bruijn^{ab,r}, J. Brunner^d, R. Bruno^a, E. Buis^{ac,r}, R. Buompane^{u,e}, J. Bustos^d, B. Caiffi^{ad}, D. Calvo^c, S. Campion^{g,ae}, A. Capone^{g,ae}, F. Carenini^{t,s}, V. Carretero^c, T. Cartraudⁿ, P. Castaldia^{af,s}, V. Cecchini^c, S. Celli^{g,ae}, L. Cerisy^d, M. Chabab^{ag}, M. Chadolias^{ah}, A. Chen^{ai}, S. Cherubini^{aj,w}, T. Chiarusi^s, M. Circella^{ak}, R. Cocimano^w, J. A. B. Coelhoⁿ, A. Coleiroⁿ, R. Coniglione^w, P. Coyle^d, A. Creusotⁿ, A. Cruz^{al}, G. Cuttone^w, R. Dallier^k, Y. Darras^{ah}, A. De Benedittis^e, B. De Martino^d, V. Decoene^k, R. Del Burgo^e, U. M. Di Cerbo^e, L. S. Di Mauro^w, I. Di Palma^{g,ae}, A. F. Díaz^j, C. Diaz^j, D. Diego-Tortosa^w, C. Distefano^w, A. Domi^{ah}, C. Donzaudⁿ, D. Dornic^d, M. Dörr^{am}, E. Drakopoulouⁱ, D. Drouhin^{b,bd}, R. Dvornický^q, T. Eberl^{ah}, E. Eckerová^{q,p}, A. Eddymaoui^m, T. van Eeden^r, M. Effⁿ, D. van Eijk^r, I. El Bojadaini^y, S. El Hedriⁿ, A. Enzenhöfer^d, G. Ferrara^w, M. D. Filipović^{an}, F. Filippini^{t,s}, D. Franciotti^w, L. A. Fusco^{z,e}, J. Gabriel^{ao}, S. Gagliardini^g, T. Gal^{ah}, J. García Méndez^l, A. Garcia Soto^c, C. Gatus Oliver^r, N. Geißelbrecht^{ah}, H. Ghaddari^y, L. Gialanella^{e,u}, B. K. Gibson^v, E. Giorgio^w, I. Goosⁿ, D. Goupilliere^o, S. R. Gozzini^c, R. Gracia^{ah}, K. Graf^{ah}, C. Guidi^{ap,ad}, B. Guillon^o, M. Gutiérrez^{aq}, H. van Haren^{ar}, A. Heijboer^r, A. Hekalo^{am}, L. Hennig^{ah}, J. J. Hernández-Rey^c, F. Huang^d, W. Idrissi Ibnsalih^e, G. Illuminati^s, C. W. James^{al}, M. de Jong^{as,r}, P. de Jong^{ab,r}, B. J. Jung^r, P. Kalaczynski^{at,be}, O. Kalekin^{ah}, U. F. Katz^{ah}, N. R. Khan Chowdhury^c, A. Khatun^q, G. Kistauri^{av,au}, C. Kopper^{ah}, A. Kouchner^{aw,n}, V. Kulikovskiy^{ad}, R. Kvavadze^{av}, M. Labalme^o, R. Lahmann^{ah}, M. Lamoureux^{bf}, G. Larosa^w, C. Lastoria^d, A. Lazo^c, E. Le Guiriec^d, S. Le Stum^d, G. Lehaut^o, E. Leonora^a, N. Lessing^c, G. Levi^{t,s}, M. Lindsey Clarkⁿ, F. Longhitano^a, J. Majumdar^r, L. Malerba^{ad}, F. Mamedov^P, J. Mańczak^c, A. Manfreda^e, M. Marconi^{ap,ad}, A. Margiotta^{t,s}, A. Marinelli^{e,f}, C. Markouⁱ, L. Martin^k, J. A. Martínez-Mora^l, F. Marzaioli^{u,e}, M. Mastrodicasa^{ae,g}, S. Mastroianni^e, S. Miccichè^w, G. Miele^{f,e}, P. Migliozzi^e, E. Migneco^w, M. L. Mitsou^e, C. M. Mollo^e, L. Morales-Gallegos^{u,e}, C. Morley-Wong^{al}, A. Moussa^y, I. Mozun Mateo^{ay,ax}, R. Muller^r, M. R. Musone^{e,u}, M. Musumeci^w, L. Nauta^r, S. Navas^{aq}, A. Nayerhoda^{ak}, C. A. Nicolau^g, B. Nkosi^{ai}, B. Ó Fearraigh^{ab,r}, V. Oliviero^{f,e}, A. Orlando^w, E. Oukachaⁿ, D. Paesani^w, J. Palacios González^c, G. Papalashvili^{au}, V. Parisi^{ap,ad}, E. J. Pastor Gomez^c, A. M. Päun^{aa}, G. E. Páválaš^{aa}, S. Peña Martínezⁿ, M. Perrin-Terrin^d, J. Perronnel^o, V. Pestel^{ay}, R. Pestesⁿ, P. Piattelli^w, C. Poire^{z,e}, V. Popa^{aa}, T. Pradier^b, S. Pulvirenti^w, G. Quéméner^o, C. Quiroz^l, U. Rahaman^c, N. Randazzo^a, R. Randriatoamanana^k, S. Razzaque^{az}, I. C. Rea^e, D. Real^c, S. Reck^{ah}, G. Riccobene^w, J. Robinson^x, A. Romanov^{ap,ad}, A. Šaina^c, F. Salesa Greus^c, D. F. E. Samtleben^{as,r}, A. Sánchez Losa^{c,ak}, S. Sanfilippo^w, M. Sanguineti^{ap,ad}, C. Santonastaso^{ba,e}, D. Santonocito^w, P. Sapienza^w, J. Schnabel^{ah}, J. Schumann^{ah}, H. M. Schutte^x, J. Seneca^r, N. Sennan^y, B. Setter^{ah}, I. Sgura^{ak}, R. Shanidze^{au}, Y. Shitov^P, F. Šimkovic^q, A. Simonelli^e, A. Sinopoulou^a, M. V. Smirnov^{ah}, B. Spisso^e, M. Spurio^{t,s}, D. Stavropoulosⁱ, I. Šteklo^P, M. Taiuti^{ap,ad}, Y. Tayalati^m, H. Tedjdit^{ad}, H. Thiersen^x, I. Tosta e Melo^{aj}, B. Trocméⁿ, V. Tsourapisⁱ, E. Tzamariudakiⁱ, A. Vacheret^o, V. Valsecchi^w, V. Van Elewyck^{aw,n}, G. Vannoye^d, G. Vasileiadis^{bb}, F. Vazquez de Sola^r, C. Verilhacⁿ, A. Veutro^{g,ae}, S. Viola^w, D. Vivolo^{u,e}, J. Wilms^{bc}, E. de Wolf^{ab,r}, H. Yepes-Ramirez^l, G. Zarpapis^t, S. Zavatarelli^{ad}, A. Zegarelli^{g,ae}, D. Zito^w, J. D. Zornoza^c, J. Zúñiga^c, and N. Zywicka^x.

^aINFN, Sezione di Catania, Via Santa Sofia 64, Catania, 95123 Italy

^bUniversité de Strasbourg, CNRS, IPHC UMR 7178, F-67000 Strasbourg, France

^cIFIC - Instituto de Física Corpuscular (CSIC - Universitat de València), c/Catedrático José Beltrán, 2, 46980 Paterna, Valencia, Spain

^dAix Marseille Univ, CNRS/IN2P3, CPPM, Marseille, France

^eINFN, Sezione di Napoli, Complesso Universitario di Monte S. Angelo, Via Cintia ed. G, Napoli, 80126 Italy

^fUniversità di Napoli "Federico II", Dip. Scienze Fisiche "E. Pancini", Complesso Universitario di Monte S. Angelo, Via Cintia ed. G, Napoli, 80126 Italy

^gINFN, Sezione di Roma, Piazzale Aldo Moro 2, Roma, 00185 Italy

^hUniversitat Politècnica de Catalunya, Laboratori d'Aplicacions Bioacústiques, Centre Tecnològic de Vilanova i la Geltrú, Avda. Rambla Exposició, s/n, Vilanova i la Geltrú, 08800 Spain

ⁱNCSR Demokritos, Institute of Nuclear and Particle Physics, Ag. Paraskevi Attikis, Athens, 15310 Greece

^jUniversity of Granada, Dept. of Computer Architecture and Technology/CITIC, 18071 Granada, Spain

^kSubatech, IMT Atlantique, IN2P3-CNRS, Université de Nantes, 4 rue Alfred Kastler - La Chantrerie, Nantes, BP 20722 44307 France

^lUniversitat Politècnica de València, Instituto de Investigación para la Gestión Integrada de las Zonas Costeras, C/ Paranimf, 1, Gandia, 46730 Spain

^mUniversity Mohammed V in Rabat, Faculty of Sciences, 4 av. Ibn Battouta, B.P. 1014, R.P. 10000 Rabat, Morocco

ⁿUniversité Paris Cité, CNRS, Astroparticule et Cosmologie, F-75013 Paris, France

^oLPC CAEN, Normandie Univ, ENSICAEN, UNICAEN, CNRS/IN2P3, 6 boulevard Maréchal Juin, Caen, 14050 France

^pCzech Technical University in Prague, Institute of Experimental and Applied Physics, Husova 240/5, Prague, 110 00 Czech Republic

^qComenius University in Bratislava, Department of Nuclear Physics and Biophysics, Mlynska dolina F1, Bratislava, 842 48 Slovak Republic

^rNikhef, National Institute for Subatomic Physics, PO Box 41882, Amsterdam, 1009 DB Netherlands

^sINFN, Sezione di Bologna, v.le C. Berti-Pichat, 6/2, Bologna, 40127 Italy

^tUniversità di Bologna, Dipartimento di Fisica e Astronomia, v.le C. Berti-Pichat, 6/2, Bologna, 40127 Italy

^uUniversità degli Studi della Campania "Luigi Vanvitelli", Dipartimento di Matematica e Fisica, viale Lincoln 5, Caserta, 81100 Italy

^vE. A. Milne Centre for Astrophysics, University of Hull, Hull, HU6 7RX, United Kingdom

- ^wINFN, Laboratori Nazionali del Sud, Via S. Sofia 62, Catania, 95123 Italy
^xNorth-West University, Centre for Space Research, Private Bag X6001, Potchefstroom, 2520 South Africa
^yUniversity Mohammed I, Faculty of Sciences, BV Mohammed VI, B.P. 717, R.P. 60000 Oujda, Morocco
^zUniversità di Salerno e INFN Gruppo Collegato di Salerno, Dipartimento di Fisica, Via Giovanni Paolo II 132, Fisciano, 84084 Italy
^{aa}ISS, Atomistilor 409, Măgurele, RO-077125 Romania
^{ab}University of Amsterdam, Institute of Physics/IHEF, PO Box 94216, Amsterdam, 1090 GE Netherlands
^{ac}TNO, Technical Sciences, PO Box 155, Delft, 2600 AD Netherlands
^{ad}INFN, Sezione di Genova, Via Dodecaneso 33, Genova, 16146 Italy
^{ae}Università La Sapienza, Dipartimento di Fisica, Piazzale Aldo Moro 2, Roma, 00185 Italy
^{af}Università di Bologna, Dipartimento di Ingegneria dell'Energia Elettrica e dell'Informazione "Guglielmo Marconi", Via dell'Università 50, Cesena, 47521 Italia
^{ag}Cadi Ayyad University, Physics Department, Faculty of Science Semlalia, Av. My Abdellah, P.O.B. 2390, Marrakech, 40000 Morocco
^{ah}Friedrich-Alexander-Universität Erlangen-Nürnberg (FAU), Erlangen Centre for Astroparticle Physics, Nikolaus-Fiebiger-Straße 2, 91058 Erlangen, Germany
^{ai}University of the Witwatersrand, School of Physics, Private Bag 3, Johannesburg, Wits 2050 South Africa
^{aj}Università di Catania, Dipartimento di Fisica e Astronomia "Ettore Majorana", Via Santa Sofia 64, Catania, 95123 Italy
^{ak}INFN, Sezione di Bari, via Orabona, 4, Bari, 70125 Italy
^{al}International Centre for Radio Astronomy Research, Curtin University, Bentley, WA 6102, Australia
^{am}University Würzburg, Emil-Fischer-Straße 31, Würzburg, 97074 Germany
^{an}Western Sydney University, School of Computing, Engineering and Mathematics, Locked Bag 1797, Penrith, NSW 2751 Australia
^{ao}IN2P3, LPC, Campus des Cézeaux 24, avenue des Landais BP 80026, Aubière Cedex, 63171 France
^{ap}Università di Genova, Via Dodecaneso 33, Genova, 16146 Italy
^{aq}University of Granada, Dpto. de Física Teórica y del Cosmos & C.A.F.P.E., 18071 Granada, Spain
^{ar}NIOZ (Royal Netherlands Institute for Sea Research), PO Box 59, Den Burg, Texel, 1790 AB, the Netherlands
^{as}Leiden University, Leiden Institute of Physics, PO Box 9504, Leiden, 2300 RA Netherlands
^{at}National Centre for Nuclear Research, 02-093 Warsaw, Poland
^{au}Tbilisi State University, Department of Physics, 3, Chavchavadze Ave., Tbilisi, 0179 Georgia
^{av}The University of Georgia, Institute of Physics, Kostava str. 77, Tbilisi, 0171 Georgia
^{aw}Institut Universitaire de France, 1 rue Descartes, Paris, 75005 France
^{ax}IN2P3, 3, Rue Michel-Ange, Paris 16, 75794 France
^{ay}LPC, Campus des Cézeaux 24, avenue des Landais BP 80026, Aubière Cedex, 63171 France
^{az}University of Johannesburg, Department Physics, PO Box 524, Auckland Park, 2006 South Africa
^{ba}Università degli Studi della Campania "Luigi Vanvitelli", CAPACITY, Laboratorio CIRCE - Dip. Di Matematica e Fisica - Viale Carlo III di Borbone 153, San Nicola La Strada, 81020 Italy
^{bb}Laboratoire Univers et Particules de Montpellier, Place Eugène Bataillon - CC 72, Montpellier Cedex 05, 34095 France
^{bc}Friedrich-Alexander-Universität Erlangen-Nürnberg (FAU), Remeis Sternwarte, Sternwartstraße 7, 96049 Bamberg, Germany
^{bd}Université de Haute Alsace, rue des Frères Lumière, 68093 Mulhouse Cedex, France
^{be}AstroCeNT, Nicolaus Copernicus Astronomical Center, Polish Academy of Sciences, Rektorska 4, Warsaw, 00-614 Poland
^{bf}UCLouvain, Centre for Cosmology, Particle Physics and Phenomenology, Chemin du Cyclotron, 2, Louvain-la-Neuve, 1349 Belgium

Acknowledgements

The authors acknowledge the financial support of the funding agencies: SC gratefully acknowledges the support from Università La Sapienza di Roma through the grant ID RM1221816813FFA3; Agence Nationale de la Recherche (contract ANR-15-CE31-0020), Centre National de la Recherche Scientifique (CNRS), Commission Européenne (FEDER fund and Marie Curie Program), LabEx UnivEarthS (ANR-10-LABX-0023 and ANR-18-IDEX-0001), Paris Île-de-France Region, France; Shota Rustaveli National Science Foundation of Georgia (SRNSFG, FR-22-13708), Georgia; The General Secretariat of Research and Innovation (GSRI), Greece Istituto Nazionale di Fisica Nucleare (INFN), Ministero dell'Università e della Ricerca (MIUR), PRIN 2017 program (Grant NAT-NET 2017W4HAT7S) Italy; Ministry of Higher Education, Scientific Research and Innovation, Morocco, and the Arab Fund for Economic and Social Development, Kuwait; Nederlandse organisatie voor Wetenschappelijk Onderzoek (NWO), the Netherlands; The National Science Centre, Poland (2021/41/N/ST2/01177); The grant “AstroCeNT: Particle Astrophysics Science and Technology Centre”, carried out within the International Research Agendas programme of the Foundation for Polish Science financed by the European Union under the European Regional Development Fund; National Authority for Scientific Research (ANCS), Romania; Grants PID2021-124591NB-C41, -C42, -C43 funded by MCIN/AEI/ 10.13039/501100011033 and, as appropriate, by “ERDF A way of making Europe”, by the “European Union” or by the “European Union NextGenerationEU/PRTTR”, Programa de Planes Complementarios I+D+I (refs. ASFAE/2022/023, ASFAE/2022/014), Programa Prometeo (PROMETEO/2020/019) and GenT (refs. CIDEGENT/2018/034, /2019/043, /2020/049, /2021/23) of the Generalitat Valenciana, Junta de Andalucía (ref. SOMM17/6104/UGR, P18-FR-5057), EU: MSC program (ref. 101025085), Programa María Zambrano (Spanish Ministry of Universities, funded by the European Union, NextGenerationEU), Spain; The European Union’s Horizon 2020 Research and Innovation Programme (ChETEC-INFRA - Project no. 101008324); Fonds de la Recherche Scientifique - FNRS, Belgium.